Volume 143 | Number 18 | 21 September 2018 | Pages 4209–4514

Analyst

rsc.li/analyst

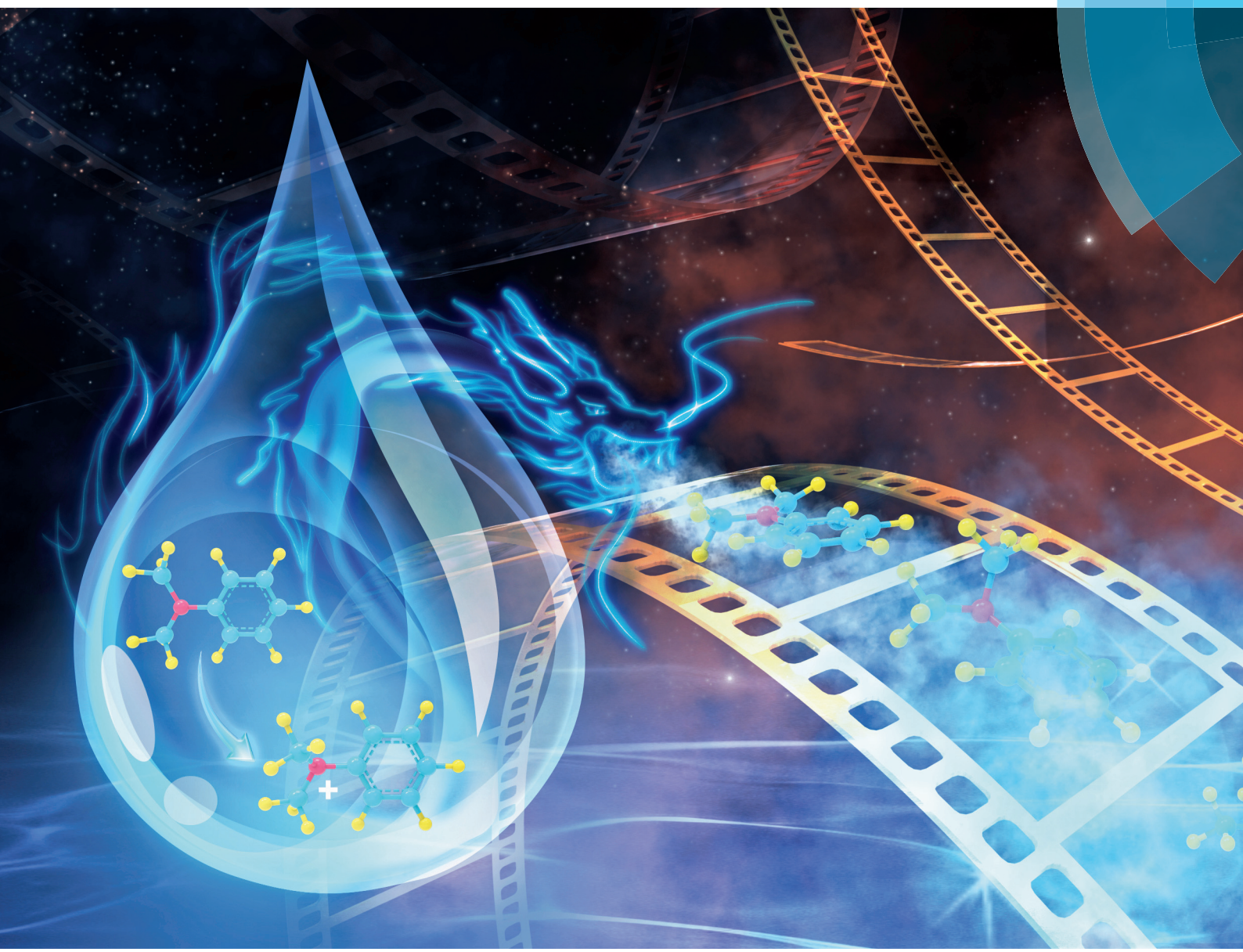

ISSN 0003-2654

ROYAL SOCIETY OF CHEMISTRY

COMMUNICATION

Jie Jiang, Richard N. Zare *et al.*

Real-time mass-spectrometric screening of droplet-scale electrochemical reactions

Analyst

COMMUNICATION

View Article Online
View Journal | View Issue

Cite this: *Analyst*, 2018, **143**, 4247

Received 24th May 2018,
Accepted 13th July 2018

DOI: 10.1039/c8an00957k

rsc.li/analyst

Real-time mass-spectrometric screening of droplet-scale electrochemical reactions†

Hong Zhang,[a] Kai Yu,[b] Na Li,[b] Jing He,[b] Lina Qiao,[a] Ming Li,[c] Yingying Wang,[b] Dongmei Zhang,[b] Jie Jiang *[b] and Richard N. Zare *[d]

A droplet-scale, real-time electrochemical reaction screening platform based on droplet spray ionization mass spectrometry (DSI-MS) has been developed. The *N*,*N*-dimethylaniline (DMA) radical cation with a half-life of microseconds was readily detected by MS during the electrooxidation of DMA, and the subsequent reactions were followed in real time for minutes.

Determining the transient intermediates generated during an electrochemical process is of prime importance to the mechanistic studies of electrochemical reactions. In many cases, one-electron[1] or multiple-electron losses[2] commonly form a very unstable radical cation. The transient reaction time of such a cation is difficult to determine. Traditional techniques that have been developed for these studies include cyclic voltammetry (CV),[3] spectroelectrochemistry,[4] and scanning electrochemical microscopy (SECM).[5–7] However, they do not provide direct chemical identification. Combining mass spectrometry (MS) with electrochemistry (EC) is appealing[8–12] owing to its capabilities for structural characterization, and its high specificity, sensitivity, and speed.

An effective interface between electrochemistry and mass spectrometry for quickly transferring electrochemically generated species from the solution to the gas phase for MS analysis is still a challenge. Since EC-MS coupling was described by Bruckenstein *et al.* in 1971,[13] various ionization methods have been applied for the online coupling of EC-MS, including thermospray,[14] fast atom bombardment (FAB),[15] electrospray ionization (ESI),[16] probe electrospray ionization,[17] nano desorption electrospray ionization (nanoDESI),[18] and differential electrochemical mass spectrometry (DEMS).[19,20] A sample transfer capillary is commonly used in these EC-MS couplings to allow the electrolytic solution to flow from electrochemical cells to ionization sources. This leads to the response times ranging from 0.1 to a few seconds.

Taking advantage of direct sampling, desorption electrospray ionization (DESI)[21,22] and easy ambient sonic-spray ionization (EASI)[23] reduce the response time to the order of milliseconds. In 2015 Zare and coworkers achieved the detection of electrogenerated short-lived intermediates by utilizing DESI to directly sample the surface of a rotating waterwheel setup[24–26] as well as a porous carbon tape with two setups (grooved inclined plane and flat plane).[27] In another study by Qiu *et al.*,[28] a hybrid ultramicroelectrode was coupled directly with a mass spectrometer and provided *in situ* information about an electrochemical reaction. However, such techniques require rather complex fabrication. The development of a simple and effective screening platform for electrogenerated species is highly desirable and would facilitate the mechanistic studies of electrochemical reactions.

The goals of the present work are (1) to develop a droplet-scale, real-time electrochemical reaction screening platform for capturing and characterizing the transient intermediates formed from an electrochemical reaction and (2) to obtain the long-time monitoring of electrochemical reaction mechanisms. This setup takes inspiration from the coupling of droplet spray ionization mass spectrometry (DSI-MS)[29] with an innovative electrochemical controlling system.

As depicted in Fig. 1, the design employs a glass slip corner positioned in front of the MS inlet, and this slip corner can be both the reservoir for the electrolyte and the spray ionization source. A three-electrode system consisting of a platinum-wire working electrode (WE), a coiled platinum counter electrode (CE), and an Ag/AgCl reference electrode (RE) is mounted on the slip corner. A potentiostat (see Fig. S1, ESI†) is used to apply a potential difference across the three electrodes to trigger both the electrochemical reaction and a spray of charged droplets. The electrodes function both as the electro-

[a]*State Key Laboratory of Urban Water Resource and Environment, Harbin Institute of Technology, Harbin 150090, China*
[b]*School of Marine Science and Technology, Harbin Institute of Technology at Weihai, Weihai 264209, China. E-mail: jiejiang@hitwh.edu.cn*
[c]*Division of Chemical Metrology and Analytical Science, National Institute of Metrology, Beijing 100029, China*
[d]*Department of Chemistry, Stanford University, Stanford, California 94305, USA. E-mail: zare@stanford.edu*

†Electronic supplementary information (ESI) available: MS/MS data for structural confirmation and experimental procedure details. See DOI: 10.1039/c8an00957k

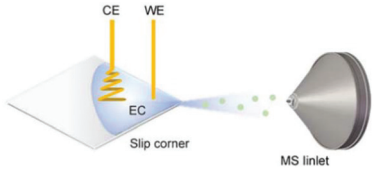

Fig. 1 Schematic representation of the droplet-scale electrochemical reaction screening setup. The reference electrode is not shown. These electrodes function both as the electrode for electrochemistry and the charging source for droplet spray.

oxidation controller and the high voltage input. The applied voltages are $E + \Delta E$ and E for the WE and CE, respectively. E is the high voltage for the charged spray and ΔE is the electrooxidation potential. In addition, the voltage of RE is $E + 0.223$ V and has no influence on the electrochemical reactions. No electrochemical oxidation or reduction is constrained to take place when the WE and CE are held at an equal high voltage ($\Delta E = 0$) (see Fig. S2, ESI†), indicating that the electrode setup works properly and has no influence on the final detection results.

Electrooxidation of aromatic amines usually gives very unstable radical cations.[1,30] One of such examples that has been extensively studied is *N*,*N*-dimethylaniline (DMA). The DMA radical cation ($DMA^{\bullet+}$) has a lifetime on the order of microseconds,[24] which is too short to be determined by conventional methods such as CV[3] and spectroscopy.[31] The well-known mechanism for the electrooxidation of DMA (Scheme 1) begins with the loss of one electron, leading to the unstable $DMA^{\bullet+}$ cation.[32] Two $DMA^{\bullet+}$ units rapidly react to yield the dimer, *N*,*N*,*N*′,*N*′-tetramethylbenzidine (TMB).[14,24] The electrooxidation then proceeds by the loss of one electron from TMB forming $TMB^{\bullet+}$ for the further generation of the trimer in the presence of excess DMA. Loss of two electrons from TMB also occurs during this reaction, which generates the quinoid TMB^{2+}.[14]

A DMA solution of 0.24 mM was prepared in acetonitrile containing 0.1 mM lithium triflate. When 20 μL of the electrolyte solution was loaded onto the glass slip corner and no potential difference was applied across the electrodes (E = 4.5 kV; ΔE = 0 V), the protonated DMA was observed at m/z 122.08 (Fig. 2a). Applying an oxidation potential of 2.0 V across the electrodes (E = 4.5 kV; ΔE = 2 V) resulted in the formation

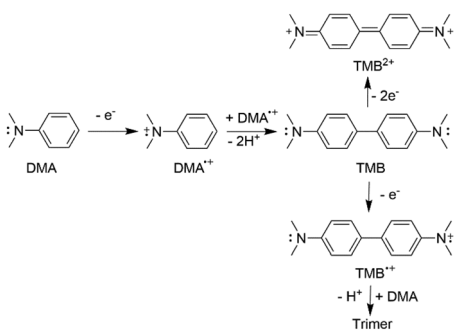

Scheme 1 Proposed electrochemical oxidation of DMA.

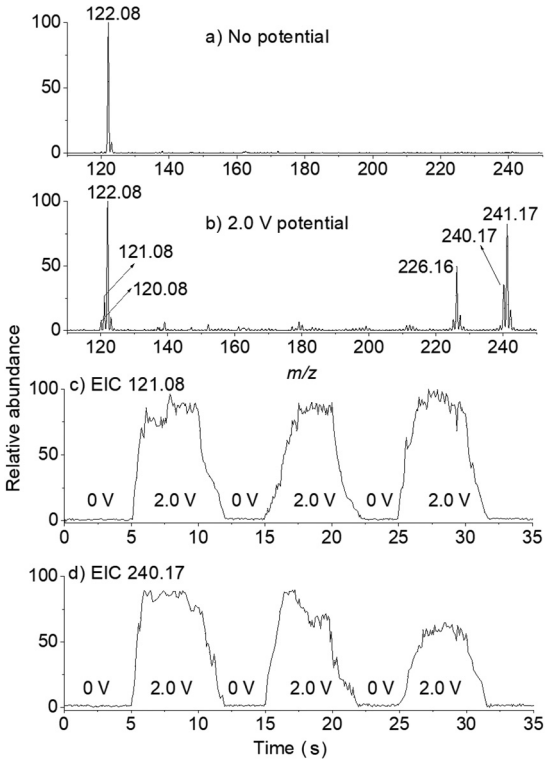

Fig. 2 Full positive-ion-mode mass spectra of DMA with (a) 0.0 V and (b) 2.0 V applied across the electrodes. EIC for the (c) 121.08 peak and (d) 240.17 peak as a function of the applied potential, which was varied between 0.0 V and 2.0 V in 5 s intervals.

of an ion at m/z 121.08, which we ascribe to the DMA radical cation intermediate (Fig. 2b). Upon CID (see Fig. S3, ESI†), the observed loss of a hydrogen atom was thought to induce the formation of a resonance stabilized aromatic imine.[24] Signals were clearly evident at m/z 241.17 and 240.17, corresponding to the protonated TMB and the radical cation of TMB. Peaks at m/z 226.16 were formed from the loss of CH_2 from $TMB^{\bullet+}$. $DMA^{\bullet+}$ and $TMB^{\bullet+}$ were both formed *via* the electrochemical oxidation of DMA, as will be shown below.

The signal intensity of $DMA^{\bullet+}$ increased greatly when an oxidizing potential was applied across the electrodes relative to when no oxidizing potential was applied, as shown in the extracted ion chromatogram (EIC) in Fig. 2c. The MS signal of $TMB^{\bullet+}$ was also markedly observed when an oxidizing potential was applied across the electrodes (Fig. 2d). Obviously, the signals of $DMA^{\bullet+}$ and $TMB^{\bullet+}$ were reproducibly observed when an oxidation potential of 2 V was applied compared to that of no oxidation potential (Fig. 2c and d). Over time, no significant decrease of $DMA^{\bullet+}$ was observed (Fig. 2c). This may be related to many factors such as short oxidation time and sufficient reactants in the solution. As shown in Fig. 2b and 3a, the peak abundances of $DMA^{\bullet+}$ and $TMB^{\bullet+}$ increased over time, indicating that these species were continually formed during the electrooxidation of DMA. This result offers direct and strong evidence for the formation of these species by DMA electrooxidation.

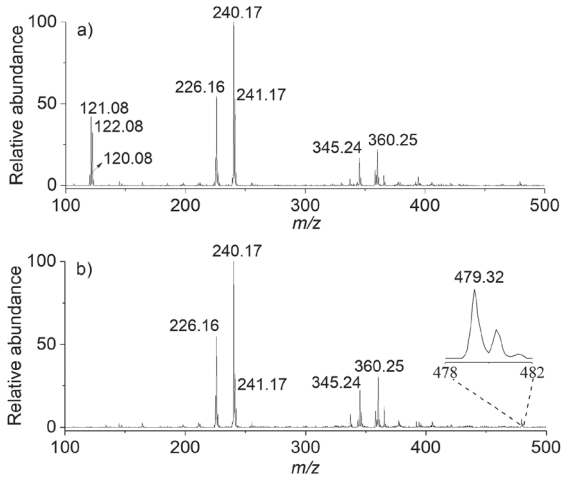

Fig. 3 Full positive-ion-mode mass spectrum of DMA electrooxidation. The mass spectra are displayed at the reaction times of (a) 20 s and (b) 90 s.

Beyond obtaining real-time information for electrochemical reactions at the initial stage, this droplet-scale electrochemistry screening approach is also applicable to the longer real-time monitoring of electrochemical reactions, limited by volatility. Fig. 3 shows the monitoring by this method for the duration of several minutes. The peak at *m*/*z* 120.08 was attributed to the quinoid TMB^{2+}. The protonated trimer (*m*/*z* 360.25) was also detected over time (Fig. 2 and 3). A comparison of the mass spectra in Fig. 3a and b shows that the peak at *m*/*z* 479.32 (protonated tetramer) was unambiguously observed (Fig. 3b inset), although it was detected at low abundance. The trimer and tetramer were also observed even when DMA was 0.024 mM (Fig. S6†), although the relative abundances showed an extent of decrease compared to the concentration of 0.24 mM (Fig. 3b and S6†). However, this contrasted with the spectrum using nESI (10 μM DMA) where no signals of the trimer and tetramer were detected.[33] Besides the concentration, this may also be related to the product transfer efficiency from the electrode surface to the spray tip for ionization. No structural information about the trimer and tetramer is available at present. However, this is the first ambient ionization mass spectrometry evidence for the observation of the quinoid TMB^{2+}, trimer, and tetramer during the electrooxidation of DMA. DMA electrochemical oxidation as a function of different electrode configurations (wire electrodes, sheet electrodes) has also been studied, and the results are presented in Fig. S4 (ESI†).

The electrooxidation of DMA with concentrations ranging from 0.024 to 2.4 mM was also investigated. As shown in Fig. S5 (ESI†), the peaks of $DMA^{\bullet+}$ were unambiguously observed at different DMA concentrations. In the present work, the great majority of DMA was converted into $DMA^{\bullet+}$ as indicated by the higher signal intensities of TMB and $TMB^{\bullet+}$ than that of the protonated DMA. In this regard, we assumed a full conversion of DMA into $DMA^{\bullet+}$ to calculate the half-life of $DMA^{\bullet+}$, although a complete conversion is impossible. Using the reported rate constant of 2.5×10^8 M^{-1} s^{-1},[6] the half-life of the observed $DMA^{\bullet+}$ was calculated to range from 1.7 to 170 μs, depending on the initial starting concentration (see Table S1, ESI†). The obtained lifetime cannot be determined by conventional methods such as SECM[6] and CV,[3] and is comparable with the results determined by DESI coupling with a water-wheel setup.[26] Compared with similar EC-MS methods,[14,17,26,28] our design has the following merits: (1) this method is simple and easy to fabricate, and can be compatible with a wide range of analysis needs. (2) By using a slip corner as the reservoir for the electrolyte as well as the spray substrate, studies of transient electrogenerated intermediates and size-dependent electrochemical reaction in a droplet are possible. (3) Because the electrolyte droplet on the corner has a capacity of 5 μL up to 60 μL, the maximum spray time can reach about 12 min, limited by solvent evaporation. In this sense, the typical solvent consumption rate is approximately 5 μL min^{-1}. Therefore, it achieves a long real-time monitoring on the scale of minutes that offers access to reaction progress and kinetics and to multiple-step reaction monitoring. (4) Replacing the slip corner with a sheet electrode can achieve high electrode surface sampling efficiency, thus facilitating the investigation of the chemical composition of an electrode–electrolyte interface.[34]

In conclusion, by coupling an innovative electrochemistry controlling system with DSI-MS, we have established a droplet-scale real-time electrochemical reaction screening platform. The short-lived DMA radical cation and products ($TMB^{\bullet+}$, quinoid TMB^{2+}, trimer, and tetramer) resulting from the electrooxidation of DMA were successfully captured and analyzed by MS. These results indicate that the isolation of electrogenerated intermediates with half-lives of milliseconds is assessable by employing a slip corner as the reservoir for both the electrolyte and spray ionization source. This platform was also compatible with a wide range of analytical needs such as different concentrations and electrode configurations. Because of the duration of the electrolyte droplet on the corner, the reaction progress on the scale of minutes was readily obtained. All these capabilities bring opportunities to perform and monitor electrochemical reaction studies *in situ*, in real time, and at a long time scale as well. Moreover, this platform has desirable features for studying more complex chemical and biological events in droplets.

Conflicts of interest

There are no conflicts to declare.

Acknowledgements

We gratefully acknowledge the Key R&D Program of Shandong Province (grant number 2016YYSP013) and the Natural Science Foundation of Shandong Province (grant number

ZR2016BM11, ZR2016BP01). R. N. Zare thanks the US Air Force Office of Scientific Research for the Basic Research Initiative Grant (AFOSR FA9550-16-1-0113).

Notes and references

1 T. Y. Zhang, S. P. Palii, J. R. Eyler and A. Brajter-Toth, *Anal. Chem.*, 2002, **74**, 1097–1103.
2 G. Dryhurst, *J. Electrochem. Soc.*, 1972, **119**, 1659–1664.
3 J. Heinze, *Angew. Chem., Int. Ed.*, 1984, **23**, 831–847.
4 Y. X. Chen, M. Heinen, Z. Jusys and R. J. Behm, *Angew. Chem., Int. Ed.*, 2006, **45**, 981–985.
5 J. L. Fernández, D. A. Walsh and A. J. Bard, *J. Am. Chem. Soc.*, 2005, **127**, 357–365.
6 F. H. Cao, J. Kim and A. J. Bard, *J. Am. Chem. Soc.*, 2014, **136**, 18163–18169.
7 S. M. Fonseca, A. L. Barker, S. Ahmed, T. J. Kemp and P. R. Unwin, *Chem. Commun.*, 2003, 1002–1003.
8 K. R. Brownell, C. C. L. McCrory, C. E. D. Chidsey, R. H. Perry, R. N. Zare and R. M. Waymouth, *J. Am. Chem. Soc.*, 2013, **135**, 14299–14305.
9 U. Karst, *Angew. Chem., Int. Ed.*, 2004, **43**, 2476–2478.
10 Z. Y. Wang, Y. Y. Zhang, B. W. Liu, K. Wu, S. Thevuthasan, D. R. Baer, Z. H. Zhu, X. Y. Yu and F. Y. Wang, *Anal. Chem.*, 2017, **89**, 960–965.
11 Y. H. Hong, Z. Y. Zhou, M. Zhan, Y. C. Wang, Y. Chen, S. C. Lin, M. Rauf and S. G. Sun, *Electrochem. Commun.*, 2018, **87**, 91–95.
12 J. C. Yu, Y. F. Zhou, X. Hua, S. Q. Liu, Z. H. Zhu and X. Y. Yu, *Chem. Commun.*, 2016, **52**, 10952–10955.
13 S. Bruckenstein and R. R. Gadde, *J. Am. Chem. Soc.*, 1971, **93**, 793–794.
14 G. Hambitzer and J. Heitbaum, *Anal. Chem.*, 1986, **58**, 1067–1070.
15 J. E. Bartmess and L. R. Phillips, *Anal. Chem.*, 1987, **59**, 2012–2014.
16 I. Iftikhar, K. M. Abou El-Nour and A. Brajter-Toth, *Electrochim. Acta*, 2017, **249**, 145–154.
17 Y. Cai, P. Y. Liu, M. A. Held, H. D. Dewald and H. Chen, *ChemPhysChem*, 2016, **17**, 1104–1108.
18 P. Y. Liu, I. T. Lanekoff, J. Laskin, H. D. Dewald and H. Chen, *Anal. Chem.*, 2012, **84**, 5737–5743.
19 H. Baltruschat, *J. Am. Soc. Mass Spectrom.*, 2004, **15**, 1693–1706.
20 J. C. P. de Souza, W. O. Silva, F. H. B. Lima and F. N. Crespilho, *Chem. Commun.*, 2017, **53**, 8400–8402.
21 Z. Takats, J. M. Wiseman, B. Gologan and R. G. Cooks, *Science*, 2004, **306**, 471–473.
22 M. Wleklinski, B. P. Loren, C. R. Ferreira, Z. Jaman, L. Avramova, T. J. P. Sobreira, D. H. Thompson and R. G. Cooks, *Chem. Sci.*, 2018, **9**, 1647–1653.
23 R. Haddad, R. Sparrapan and M. N. Eberlin, *Rapid Commun. Mass Spectrom.*, 2006, **20**, 2901–2905.
24 T. A. Brown, H. Chen and R. N. Zare, *Angew. Chem., Int. Ed.*, 2015, **54**, 11183–11185.
25 T. A. Brown, N. Hosseini-Nassab, H. Chen and R. N. Zare, *Chem. Sci.*, 2016, **7**, 329–332.
26 T. A. Brown, H. Chen and R. N. Zare, *J. Am. Chem. Soc.*, 2015, **137**, 7274–7277.
27 H. Cheng, X. Yan and R. N. Zare, *Anal. Chem.*, 2017, **89**, 3191–3198.
28 R. Qiu, X. Zhang, H. Luo and Y. H. Shao, *Chem. Sci.*, 2016, **7**, 6684–6688.
29 J. Jiang, H. Zhang, M. Li, M. T. Dulay, A. J. Ingram, N. Li, H. You and R. N. Zare, *Anal. Chem.*, 2015, **87**, 8057–8062.
30 G. J. Van Berkel, K. G. Asano and V. Kertesz, *Anal. Chem.*, 2002, **74**, 5047–5056.
31 W. Kaim and J. Fiedler, *Chem. Soc. Rev.*, 2009, **38**, 3373–3382.
32 H. Yang, D. O. Wipf and A. J. Bard, *J. Electroanal. Chem.*, 1992, **331**, 913–924.
33 Q. Wan, S. Chen and A. K. Badu-Tawiah, *Chem. Sci.*, 2018, **9**, 5724–5729.
34 J. S. Lu, X. Hua and Y. T. Long, *Analyst*, 2017, **142**, 691–699.

